Fuel Processing Technology 205 (2020) 106431

Contents lists available at ScienceDirect

Fuel Processing Technology

journal homepage: www.elsevier.com/locate/fuproc

Research article

Exploring the microscopic reaction mechanism of H_2S and COS with CuO oxygen carrier in chemical looping combustion

Chaohe Zheng, Haibo Zhao*

State Key Laboratory of Coal Combustion, Huazhong University of Science and Technology, Wuhan 430074, PR China

ARTICLE INFO

Keywords:
Chemical looping
Density functional theory (DFT)
Cu-based oxygen carrier
H_2S and COS
Adsorption and dissociation

ABSTRACT

Density functional theory (DFT) calculations are employed to investigate the reaction mechanisms of H_2S or COS with CuO in this work, including the microscopic adsorption, dissociation, and further reactions over the perfect (fresh) and defect (partially reduced) CuO (111) surfaces. On the perfect surface, the elementary reaction of $HS^* \rightarrow H^* + S^*$ is the rate-determining step in the two-step H_2S dissociation process, and the formation of H_2O is however the rate-determining step for the whole reaction between H_2S and CuO. As for the defect surface, the reaction of H_2O formation is still a more preferable pathway than the complete dissociation and H_2 formation route. In view of COS decomposition on the perfect surface, the energy barriers for the formation of CO or CO_2 from COS decomposition are too high, and thus are difficult to take place. On the defect surface, the presence of oxygen vacancy greatly promotes the adsorption and subsequent decomposition of COS. Finally, the remaining sulfur favorably exists on the surface rather than SO_2 formation, and copper sulfides will inevitably generate as the dissociations of H_2S or COS proceed. The results attained in this work are helpful to give insights into the sulfur evolution of sulfur-containing fuels in the chemical looping combustion process.

1. Introduction

Chemical looping combustion (CLC), with the characteristic of inherent CO_2 separation during fossil fuel conversion process, has been proposed as a promising way to address the global warming issue [1–4]. There are two reactors in the CLC system, *i.e.*, air reactor (AR) and fuel reactor (FR). Oxygen carrier (OC), as known as the heat and oxygen medium, is used to bridge the reactions in the two reactors, which is deemed as a key component in CLC. Cu-based materials have been regarded as suitable OC candidates due to its excellent reactivity, high oxygen transport capacity, and relatively low costs [5–7].

Nevertheless, Cu-based OC is generally sulfur-sensitive, and its performance (reactivity, durability, and resistance to sintering/agglomeration) can be easily degraded by the sulfidation of sulfur-containing species in the reacting atmosphere. The fate of sulfur in the continuously operated CLC units has been extensively investigated by using various fuel and sulfur concentrations [8–15]. It was verified that H_2S and COS are the main sulfur-containing species in the coal pyrolysis and subsequent char gasification process during *in-situ* gasification chemical looping combustion (*i*G-CLC) [8]. On the Cu-based OC side, the main sulfide product is Cu_2S within the CLC operation temperature window [9–13]. It was found that a high H_2S concentration favored the growth of Cu_2S [16]. Furthermore, the regeneration characteristics between copper sulfides and copper oxides were also investigated, and a high concentration of SO_2 was detected from the exhaust of the AR [14,17]. Adánez et al. [10,12] showed that the sulfur can be transferred into the chemical-looping system, and then released as SO_2 in the AR, while Pachler et al. [15] found that SO_2 could merely be detected in the FR exhaust gas stream rather than in the AR. As can be expected, the SO_2 emission behaviors should be very different in the AR or the FR, which corresponds to the oxygen-rich or oxygen-poor atmosphere, respectively. Therefore, in order to make clear the sulfidation reactions as well as the regeneration reactions in the realistic CLC process, the interactions between sulfur-containing species (H_2S and COS) and CuO should be systematically investigated separately first.

Actually, the sulfidation of copper oxides by H_2S may occur via different pathways [10,11]. Both Cu_2S and SO_2 can be produced from sulfur species, while H_2 and H_2O mainly derive from the dehydrogenation of H_2S, and CO and CO_2 are the possible products from COS decomposition. That is, the fate of hydrogen or sulfur is still ambiguous in the previous literatures. Therefore, gaining insights into the interaction and reaction pathways of H_2S and COS with CuO is urgently required.

Density functional theory (DFT) method has been widely used to calculate the adsorption, dissociation, and relevant theoretical reaction pathways of various molecules on the CuO (111) surface [18–21]. More

* Corresponding author.
E-mail address: hzhao@mail.hust.edu.cn (H. Zhao).

https://doi.org/10.1016/j.fuproc.2020.106431
Received 6 January 2020; Received in revised form 26 March 2020; Accepted 30 March 2020
Available online 20 April 2020
0378-3820/

recently, DFT calculations have been successfully employed to explore the microscopic adsorption and dissociation mechanisms of H_2S with the commonly used OC materials in CLC, *i.e.*, the Cu_2O (111) surface [22], the CuO (111) surface [23,24], the Fe_2O_3 (0001) surface [25,26], and the NiO (001) surface [27] et al. Sun et al. [23] firstly investigated the adsorption and dissociation mechanism on the perfect CuO (111) surface, and Zhang et al. [24] then successively calculated the adsorptions and dissociation pathways of H_2S on the stoichiometric, reduced, and sulfurized CuO (111) surfaces at 475 K. Song et al. [25] investigated the interactions between H_2S and α-Fe_2O_3 (0001), and concluded that α-Fe_2O_3 not only served as a catalyst to accelerate the dissociation of H_2S to form H_2 and S via the H_2-forming path, but also acted as one reactant to participate in the reaction of H_2O-forming path. Similarly, over the ZnO (1010) surface, H_2O-forming path was proved to be more favorable than the H_2-forming path [28]. However, fundamental insights into the sub-steps of the interaction between H_2S and CuO, such as the possible products and relevant reaction pathways on the Cu-based surface, are still lack.

The recently investigated interactions between COS and CuO mainly include hydrogenation, hydrolysis, and direct reactions. Among these reactions, the hydrolysis of COS has gained growing concerns in the several experimental [29–31] and DFT calculation studies [32–34]. However, within the CLC operation temperatures range, the hydrolysis reaction is not so important in determining the COS concentration, but rather the direct reaction between COS and CuO [13,35]. On the other hand, by means of the underlying reaction pathways of the direct reaction between COS and CuO, it will be beneficial to provide qualitative and quantitative insights into the understanding of the hydrogenation or hydrolysis reaction mechanisms. Gao et al. [36] applied DFT investigations to explore the reaction of atomic Cu^+ with COS, and indicated the C—S bond cleavage is energetically much more favorable than the C—O bond cleavage. Nevertheless, up to date, there is no report on the direct reaction between COS and CuO.

In the FR of the real CLC conditions, the OCs will be reduced by the fuel, resulting in the generation of oxygen vacancies and the formation of the partially reduced CuO surface, which might exhibit different reaction properties from the perfect surface [20,37]. Hence, both perfect (fresh) and defect (partially reduced) CuO surfaces are chosen for the investigations in this study. The objective of this work is to explore the reaction mechanisms of H_2S or COS with CuO by the DFT calculation method. The adsorption and dissociation of H_2S and COS on the perfect or defect surfaces are explored, which reflect the detailed interaction information and the rate-limiting step on the basis of energy barrier analyses. These fundamental insights can be beneficial to the holistic understanding of the reaction mechanism of the sulfur evolution behaviors over the Cu-based OC in the chemical-looping system.

2. Computational details

All DFT calculations are conducted by the CASTEP (Cambridge Serial Total Energy Package) [38,39] program. The generalized gradient approximation (GGA) [38] in the form of Perdew-Wang (PW91) is adopted for the electron exchange-correlation energy. The interactions of electron and ion are modeled by ultra-soft pseudo-potential. A Monkhorst-Pack mesh of 5 × 7 × 5 and 3 × 2 × 1 for CuO cell and CuO slab is used, and the cutoff energy is 400 eV [40,41]. The Hubbard parameter U is introduced to describe the strong electron correlations of transition metals according to the well-known GGA + U method [42], and 7.5 eV is set as a reasonable U value for the Cu 3d orbitals [40,41,43,44]. The van der Waals-inclusive correction (DFT-D) with the Ortmann-Bechstedt-Schmidt (OBS) method is applied in this study.

For the calculations, the CuO cell is optimized first, as shown in Fig. 1a. The lattice parameters of the CuO cell (a = 4.653 Å, b = 3.410 Å, c = 5.108 Å, and β = 99.50°) are in good agreement with experimental values (a = 4.682 Å, b = 3.424 Å, c = 5.127 Å, and β = 99.42°) [45]. A six-layer p (2 × 3) CuO (111) slab model is then constructed, while the top three layers are relaxed and the bottom three layers are fixed in the calculations. The vacuum space is 15 Å, and the convergence criterion for the total energy is 1.0 × 10^{-5} eV/atom, while the maximum interatomic force and displacement are 0.03 eV/Å and 0.001 Å, respectively. All molecules are optimized in a 20 Å × 20 Å × 20 Å periodic cubic vacuum box, and the results of parameter tests can be found in Section S1 in Supplemental Material (SM).

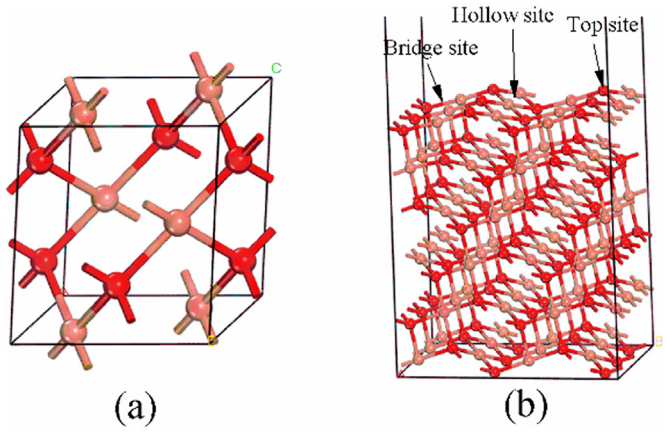

Fig. 1. Microstructures of (a) CuO bulk cell; (b) six-layer CuO (111) slab model.

To investigate the interaction between the slab and sulfur-containing species, the adsorption energy is defined as:

$$E_{ads} = E(A) + E(B) - E(AB) \quad (1)$$

where $E(AB)$, $E(A)$, and $E(B)$ refer to the total energies of the adsorption structure, the substrate, and the adsorbate, respectively. Moreover, complete LST/QST (linear/quadratic synchronous transit) approach is used to calculate the energy barrier, E_b, of different reaction steps, which is defined as:

$$E_b = E(TS) - E(IS) \quad (2)$$

where E(TS) and E(IS) are the energies of the transition state and the initial state, respectively.

3. Results and analysis

3.1. Adsorption of COS, H_2S, HS*, and atomic S*, H* species

The adsorptions of COS, H_2S, and resultant dissociated HS*, S*, H* species on the CuO (111) surface have been examined. On the perfect surface, two adsorption modes (perpendicular or parallel) and three adsorption sites (Top site, Bridge site, Hollow site) are considered; while on the defect surface, oxygen vacancy sites are further considered. It is stressed here that T_{Cu3f} site represents three-fold coordinated top copper site, $B_{Cu3f\text{-}Cu3f}$ site represents the bridge bond between two three-fold coordinated copper atoms, and $H_{O3f\text{-}O3f\text{-}Cu3f\text{-}Cu3f}$ site represents the hollow between these four atoms (O_{3f}, O_{3f}, Cu_{3f}, and Cu_{3f}). Other adsorption sites have the analogous nomination, which will not be expressed later. The optimized geometric structures and the corresponding adsorption energies of H_2S, HS*, S*, H* and COS on the perfect and defect surfaces are shown in Fig. 2.

3.1.1. H_2S adsorption

For the H_2S adsorption on the perfect CuO surface, 18 configurations (as shown in Fig. S2 of SM) have been constructed to explore the most stable adsorption structure. H_2S molecule is placed perpendicular or parallel to nine sites (Top sites T_{O3f}, T_{O4f}, T_{Cu3f}, T_{Cu4f}, Bridge sites $B_{O3f\text{-}O3f}$, $B_{Cu3f\text{-}Cu3f}$, $B_{O4f\text{-}O4f}$, $B_{Cu4f\text{-}Cu4f}$, and Hollow site $H_{O3f\text{-}O3f\text{-}Cu3f\text{-}Cu3f}$). After geometry optimization, it can be found in Fig. 2a (H_2S*) that the configuration where H_2S parallels to the T_{Cu3f}site is the most stable

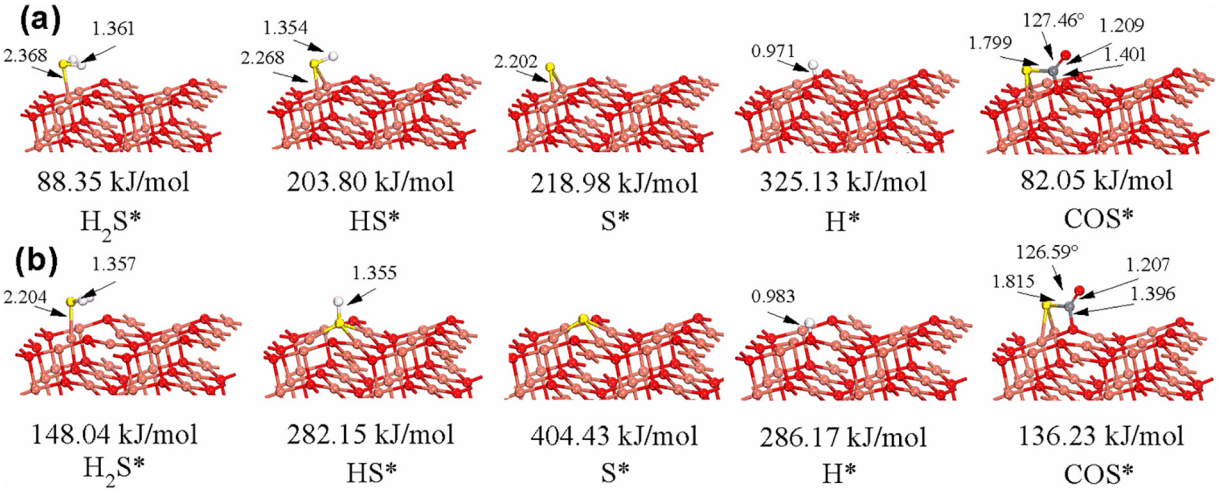

Fig. 2. The optimized geometric structures of H_2S*, HS*, S*, H* and COS* adsorptions on (a) the perfect surface and (b) the defect surface, and '*' represent the adsorbed state. (Yellow ball: S, White ball: H, Red ball: O, Salmon pink ball: Cu, Grey ball: C.) (For interpretation of the references to colour in this figure legend, the reader is referred to the web version of this article.)

geometric adsorption (with the largest adsorption energy) among the 18 different configurations. The adsorption energy (88.35 kJ/mol) is in line with the previous results (88.0 kJ/mol) [24], and the bond lengths of S—Cu and H—S are 2.368 Å and 1.361 Å, respectively.

Furthermore, three configurations of H_2S adsorption on the defect surface are then examined based on the above results (Fig. S3 of SM). As shown in Fig. 2b (H_2S*), H_2S still chemisorbs at T_{Cu3f} site near the oxygen vacancy. The adsorption energy (148.04 kJ/mol) is in line with the previous results (143.5 kJ/mol) [24]. The bond lengths of S—Cu and H—S are 2.268 Å and 1.354 Å, respectively. Thus, the above two structures are set as the initial states of the H_2S dissociation on the perfect and defect surfaces, respectively.

3.1.2. HS* adsorption

In the case of HS* adsorption on the perfect surface, the HS* species is perpendicular or parallel to eight sites (Top sites T_{O3f}, T_{O4f}, T_{Cu3f}, T_{Cu4f}, Bridge sites $B_{O3f\text{-}O3f}$, $B_{Cu3f\text{-}Cu3f}$, $B_{O4f\text{-}O4f}$, and $B_{Cu4f\text{-}Cu4f}$). The results indicate that the configuration where HS* parallels to the $B_{Cu3f\text{-}Cu3f}$site is the most stable structure, and the adsorption energy is 203.80 kJ/mol. As for the defect surface, the sulfur atom of HS* species moves downward to fully immerse into the oxygen vacancy site, and bonds tightly with three adjacent copper atoms. The bond length of H—S is 1.355 Å, and the adsorption energy is 282.15 kJ/mol.

3.1.3. S* adsorption

With regard to S* adsorption, S* atom is perpendicular or parallel to eight sites (Top sites T_{O3f}, T_{O4f}, T_{Cu3f}, T_{Cu4f}, Bridge sites $B_{O3f\text{-}O3f}$, $B_{Cu3f\text{-}Cu3f}$, $B_{O4f\text{-}O4f}$, and $B_{Cu4f\text{-}Cu4f}$). It is found that sulfur tends to adsorb at the $B_{Cu3f\text{-}Cu3f}$site on the perfect surface, while at the oxygen vacancy site on the defect surface. The adsorption energies are 218.98 kJ/mol and 404.43 kJ/mol, respectively, which are in line with previous study [23,24].

3.1.4. H* adsorption

With respect to H* adsorption, H* atom is perpendicular or parallel to four top sites (T_{O3f}, T_{O4f}, T_{Cu3f}, and T_{Cu4f}). It is noted that H* atom always prefers to adsorb at the T_{O3f}site with a distance of 0.971 Å, on both the perfect and defect surfaces. And the adsorption energy (325.13 kJ/mol) agrees well with previous results [23].

3.1.5. COS adsorption

15 geometrical configurations of COS adsorption on the perfect surface have been considered in this work. As shown in Fig. S4 of SM, COS molecule is perpendicular to sites (Top sites T_{O3f}, T_{O4f}, T_{Cu3f}, T_{Cu4f}, Bridge sites $B_{O3f\text{-}O3f}$, $B_{Cu3f\text{-}Cu3f}$, and Hollow site $H_{O3f\text{-}O3f\text{-}Cu3f\text{-}Cu3f}$), and parallel to sites (Bridge sites $B_{O3f\text{-}O3f}$, $B_{Cu3f\text{-}Cu3f}$, $B_{O4f\text{-}O4f}$, $B_{Cu4f\text{-}Cu4f}$, $B_{O3f\text{-}Cu3f}$, and Hollow sites $H_{O4f\text{-}O4f\text{-}O3f\text{-}O3f}$, $H_{Cu3f\text{-}Cu3f\text{-}O3f\text{-}O3f}$, $H_{O4f\text{-}O4f\text{-}Cu3f\text{-}Cu3f}$). After geometry optimization, the configuration where COS parallels to the $H_{Cu3f\text{-}Cu3f\text{-}O3f\text{-}O3f}$ site is found to be the most stable adsorption. As seen in Fig. 2a (COS*), S atom adsorbs at the $B_{Cu4f\text{-}Cu4f}$ site, and the C atom migrates from the initial $B_{O3f\text{-}O3f}$ site to T_{O3f} site, while the O atom slightly raises away from surface. Meanwhile, the angle of O-C-S is 127.46°, and the bond lengths of C—O and C—S are 1.209 Å and 1.799 Å, respectively, which are longer than the free bond lengths (1.181 Å and 1.558 Å), indicating that the adsorption weakens the interactions between these atoms.

Analogously, three placement types of COS on the defect surface are calculated (as shown in Fig. S6 of SM), and the most stable structure is shown in Fig. 2b (COS*). The adsorption free energy is 136.23 kJ/mol, which is apparently higher than that of the perfect surface (82.05 kJ/mol), indicating that the adsorption is strongly promoted by the presence of oxygen vacancy. The angle of O-C-S is 126.59°, and the bond lengths of C—O and C—S are 1.207 Å and 1.815 Å, respectively. Therefore, the above two structures are set as the initial state of the COS dissociation on the perfect and defect surfaces, respectively.

3.2. The dissociation and further reaction of H_2S on the perfect surface

To characterize the interaction between H_2S and CuO, the initial dissociation process of the H_2S over the CuO (111) surface is rather essential. The potential energy diagram for H_2S dissociation and further reactions over the perfect CuO surface is shown in Fig. 3, together with the corresponding configurations. As mentioned above, the configuration of H_2S adsorption in Fig. 2a (H_2S*) is set as the initial state ('H_2S*' in Fig. 3) of H_2S dissociation. The gradual dehydrogenations of H_2S (H_2S* → HS* + H* and HS* → H* + S*) are firstly examined. In the first dehydrogenation step, the adsorbed H_2S* is dissociated spontaneously into HS* and H* with an energy barrier of 4.82 kJ/mol at TS1, in which S* bonds with two adjacent Cu atoms ('HS* + H*' in Fig. 3). Subsequently, the second dehydrogenation step occurs by overcoming an energy barrier of 26.05 kJ/mol at TS2, and as depicted in Fig. 3 (S* + 2H*), the adsorbed S* is formed while two H* adsorb at two different T_{O3f} sites. Furthermore, the energy barrier of the first (4.82 kJ/mol) and second (26.05 kJ/mol) dehydrogenation steps are similar with previous studies of 2.4 and 23.1 kJ/mol [23] and 9.1 and 28.6 kJ/mol [24], respectively. Note that, the energy barrier for the first dehydrogenation step is significantly lower than that of the second step, suggesting that the reaction of HS* → H* + S* is the rate-

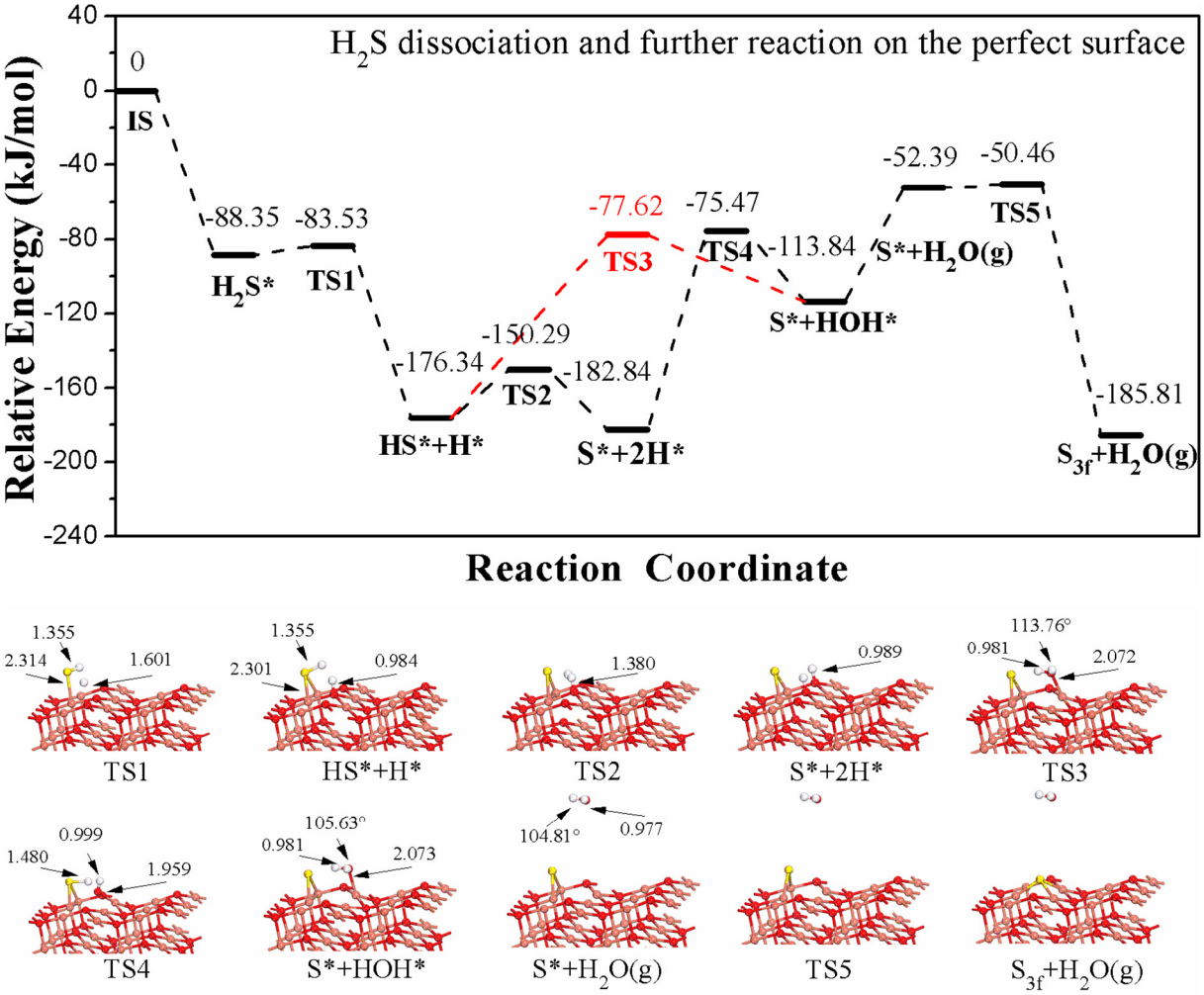

Fig. 3. Potential energy profiles and the corresponding structures of H_2S dissociation and further reactions on the perfect CuO surface.

determining step in the two-step dehydrogenation process.

According to the reaction of CuO + H_2S → Cu_xS + H_2O, the further reactions of H_2O generation and sulfur evolution are also considered as a significant step to reveal the entire reaction process of the interaction between H_2S and CuO. As shown in Fig. 3 (S* + HOH*), one H* atom (separated from one (O—H)* group) migrates to the other T_{O3f} site, and forms a (H-O-H)* structure chemically bonded to the T_{Cu4f} site with an energy barrier of 107.37 kJ/mol at TS4, which can release as gaseous H_2O at a distance of 6 Å above the surface. Nevertheless, considering that the HS* in the microstructure of 'TS4' is similar to the one in the configuration of 'HS* + H*', the transition state from 'HS* + H*' to 'S* + HOH*' is thus searched and the corresponding structure is depicted in Fig. 3 (TS3). The energy barrier (98.72 kJ/mol at TS3) is slightly lower than that at TS4 (107.37 kJ/mol), indicating that the reaction of HS* + H* + CuO → (HOH)* + CuO_{x-1} might be a more preferable pathway to form a (H-O-H)* group than the reaction of 2H* + CuO → (HOH)* + CuO_{x-1}. In this sense, the formation of H_2O might be difficult to occur for the entirely dissociated configurations (namely 'S + 2H*').

Besides, the H_2 formation in the whole process has been inspected. The configurations of 'H_2S*', 'HS* + H*', and 'S* + 2H*' in Fig. 3 are set as the initial states in Fig. 4, and the configuration where gaseous H_2 molecule is placed above the surface with a distance of 5 Å is set as the final state of H_2 formation. The energy barriers for three pathways are 222.88 kJ/mol, 270.76 kJ/mol, and 237.18 kJ/mol, respectively. In comparison with the energy barriers of H_2S dissociation and H_2O formation, it can be concluded that H_2O formation is quite easier to proceed than that of H_2 formation.

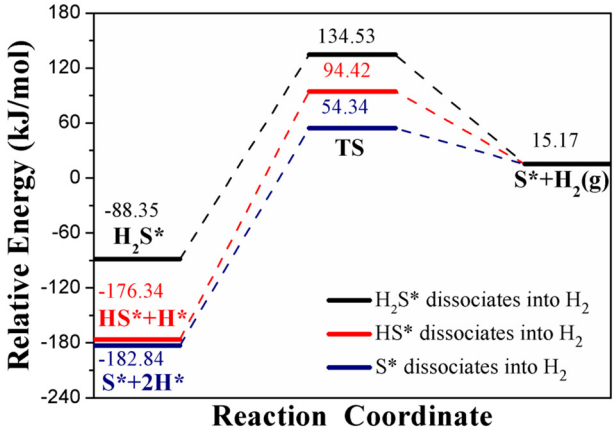

Fig. 4. Potential energy profiles of H_2 formation on the CuO surface.

It is noted that two pathways of H_2O formation in Fig. 3 could both contribute to the release of gaseous H_2O and the formation of oxygen vacancy ('S* + H_2O(g)' in Fig. 3), and the desorption is endothermic by 61.45 kJ/mol. This value is obviously lower than the H_2O desorption free energy (75.27 kJ/mol) [46], implying that the desorption process of H_2O or namely the formation of oxygen vacancy can be facilitated in the presence of sulfur. According to the Lewis acid-base theory [47], the removal of an oxygen atom from the CuO surface will leave behind two

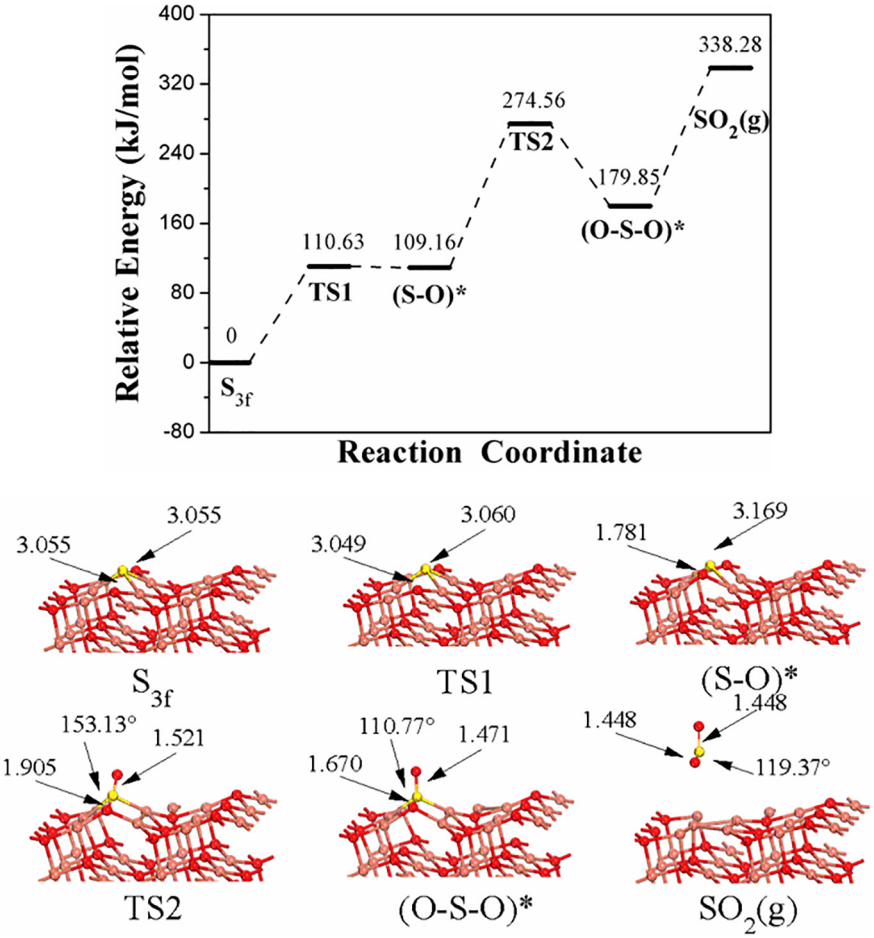

Fig. 5. Potential energy profiles of SO_2 formation and the corresponding structures.

unpaired electrons. This implies that the oxygen vacancy is a strong Lewis base, and the active S* will migrate onto the oxygen vacancy and form a strong adsorption structure like S_{3f} site (three-fold coordinated sulfur site) in the final state ('S_{3f} + H_2O(g)' in Fig. 3) with a very low energy barrier of 1.93 kJ/mol. On the contrary, the adsorption of S* at the oxygen vacancy is extremely high (404.43 kJ/mol). In this sense, H_2S eventually dissociates into H_2O molecule and the residual S* remains stably in the surface.

As known, the fate of sulfur might also lead to the generation of SO_2, and the pathways of SO_2 formation via the reaction between S_{3f} and surface lattice oxygen are then identified. It can be seen in Fig. 5 that the SO_2 formation process proceeds through a three-step process in the sequence of S initial oxidation (S* → (S—O)*) → S secondary oxidation ((S—O)* → (O-S-O)*) → SO_2 desorption ((O-S-O)* → SO_2(g)). The surface slab in the configuration of 'S_{3f} + H_2O(g)' in Fig. 3 is chosen as the initial state of SO_2 formation (Fig. 5 (S_{3f})). In the initial oxidation step (S* → (S—O)*), the surface S* atom is oxidized by a three-fold coordinated lattice oxygen to produce a (S—O)* structure with an energy barrier of 110.63 kJ/mol, and this process requires 109.16 kJ/mol of heat. In the secondary oxidation step ((S—O)* → (O-S-O)*), the formed (S—O)* structure combines with another lattice oxygen atom and produce a (O-S-O)* structure. This oxidation step is a strongly endothermic reaction (70.69 kJ/mol) with an energy barrier of 165.40 kJ/mol. Finally, the SO_2 molecule desorbs from the surface, and three defect sites are then generated after SO_2 desorption. The desorption process is endothermic by 158.43 kJ/mol. The energy barrier of the first oxidation step is significantly lower than that of the second step, suggesting that the reaction of (S—O)* → (O-S-O)* is the rate-determining step in the three-step SO_2 formation process. However, it is noted that the energy barriers of three-step S oxidation might be too high, and thus be difficult to take place under an O_2-free condition.

3.3. The dissociation and further reaction of H_2S on the defect surface

To characterize the H_2S dissociation and further reaction on the defect surface, the minimum free energy path of H_2S gradual dehydrogenation is firstly examined. It can be seen in Fig. 6 that the elementary reaction of H_2S* → HS* + H* is exothermic by 95.61 kJ/mol, with an energy barrier of 26.89 kJ/mol at TS1. The elementary reaction of HS* → HS_{3f} is exothermic by 6.64 kJ/mol with a small activation energy of 0.26 kJ/mol at TS2. The energy barriers at TS1 (26.89 kJ/mol) and TS2 (0.26 kJ/mol) are in line with the previous values (20.0 kJ/mol and 0.60 kJ/mol, respectively) [24].

As it can be seen in Fig. 6, the configurations of 'HS* + H*' is similar to the co-adsorption of two H atoms on the sulfur-containing surface (like 'S_{3f}' shown in Fig. 5). That is, one H atom adsorbs at T_{O3f} site and the other H atom adsorbs at T_{S3f} site. Hence, in view of the substep reaction, the H atom of HS* species is separated from the original T_{S3f} site and then placed close to the nearby two possible T_{O3f} sites, forming (O—H)* or (H-O-H)* groups, which correspond to the configurations of 'S_{3f} + 2H*' and 'S_{3f} + HOH*' shown in Fig. 6.

As for pathway 1 (S_{3f} + H* → S_{3f} + 2H*, indicated by the red line in Fig. 6): with H—S bond cleavage, H atom (derived from HS*) moves to the clean T_{O3f} site which bonds without H*, forming a similar structure as shown in Fig. 6 (S_{3f} + 2H*). The bond length of H—O is 0.982 Å, which is equal to the former H—O bond length. The energy barrier of this elementary step is 40.75 kJ/mol at TS3, and the reaction is strongly exothermic by 86.07 kJ/mol. The lowest overall energy

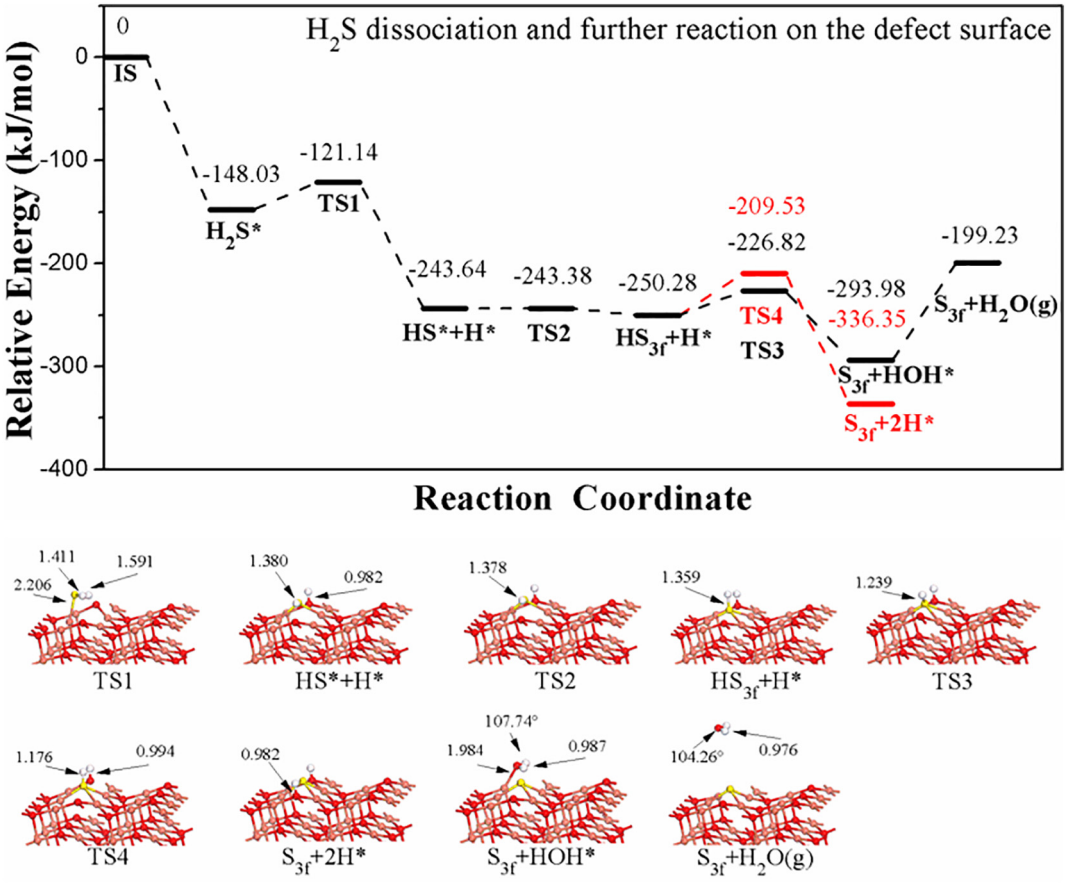

Fig. 6. Potential energy profiles and the corresponding structures of H_2S dissociation and further reactions on the defect CuO surface.

(−336.35 kJ/mol) indicates the thermodynamical stability of this structure as well.

As for pathway 2 (S_{3f} + H* → S_{3f} + HOH*): similarly, H* atom separates from the original T_{S3f} site to the nearby T_{O3f} site which bonds to the other H* atom, and a new (H-O-H)* structure is produced, as depicted in Fig. 6 (S_{3f} + HOH*). The angle of (H-O-H)* is 107.74°, and two H−O bond have the same length of 0.987 Å. The elementary reaction is exothermic by 43.70 kJ/mol, with a small energy barrier of 23.46 kJ/mol at TS4. Finally, the desorption energy of H_2O is 94.75 kJ/mol. In comparison to pathway 1, the relatively lower energy barrier (23.46 kJ/mol vs 40.75 kJ/mol) indicates that pathway 2 is kinetically more favorable.

3.4. The dissociation of COS on the perfect surface

In terms of the dissociation of COS, both C−S and C−O bond cleavages are considered. For the C−O bond cleavage, the migration paths of O atom to the neighbor T_{Cu4f} or T_{O3f} sites are considered. It is noted that in the two migration paths, O atom tends to move back to the initial state to form an original structure like Fig. 7 (COS*), suggesting that the C−O bond cleavage is difficult to occur. As for the C−S bond cleavage, there are also two paths for the C−O group to migrate to, *i.e.*, T_{Cu3f} or T_{O3f} sites. Interestingly, it can be seen that the (C−O)* group bonding to a surface copper atom is similar to the geometric configuration of CO adsorption, while the latter one would lead to the formation of (O-C-O)* group. Therefore, the above two stable geometric configurations are chosen as the final states for path 1 (S + COO*) and path 2 (S + CO*) in Fig. 7, which corresponds to the formation of CO and CO_2 from COS decomposition, respectively. Additionally, the calculation results also hint that the C−S bond cleavage is energetically much more favorable than the C−O bond activation, which agrees with previous study [36].

Path 1 (COS dissociates into CO_2(g), black line): as the bond length of S−C is stretched from 1.8 Å to 3.0 Å and the (C−O)* group is merely bonding to T_{O3f} site, it spontaneously forms an (O-C-O)* structure, and the lattice oxygen (of origin T_{O3f} site) is pulled out from the surface. The angle of the (O-C-O)* is 178.61°, and the distance between C (of CO) and T_{Cu4f} (adjacent copper site) is 3.027 Å. The transient state of this step is presented in Fig. 7 (TS1). The Cu−S bond lengths are 1.200 and 1.336 Å, and the angle of the (O-C-O)* is 133.90°. The energy barrier of this elementary process is 83.53 kJ/mol, and it is endothermic by 34.74 kJ/mol. The higher energy barrier (than the adsorption energy of COS) indicates that the generation of CO_2 is neither thermodynamically nor kinetically favorable. Subsequently, in view of the desorption of CO_2, as shown in Fig. 7 (FS), the (O-C-O)* group moves to above the surface with a distance of 5 Å. The angle of O-C-O (179.65°) and the bond length of C−O (1.182 Å) are in line with the values of free CO_2 (180° and 1.180 Å). The desorption of CO_2 is slightly endothermic. As a result, a reduced surface like the slab model shown in Fig. 3 (S_{3f} + H_2O (g)) is produced, and the residual S* will also be inevitably remained at the oxygen vacancy.

Path 2 (COS dissociates into CO(ads), red line): with the S−C bond cleavage, the (C−O)* group migrates and then bonds to the T_{Cu3f} site, and a configuration of CO adsorption is thus produced. This elementary step is a strongly endothermic process (119.10 kJ/mol) with an energy barrier of 205.51 kJ/mol at TS2. Such a high energy barrier implies that the decomposition of COS to form CO has no thermodynamic or kinetic advantages. In view of the subsequent oxidation of CO, as shown in Fig. 7 (S* + COO*), CO interacts with the surface lattice oxygen, and forms a linear CO_2 complex which bonds with a copper atom. The energy barrier of CO oxidation in the presence of S* is 64.16 kJ/mol at TS3, which is prominently higher than the calculated energy barrier of

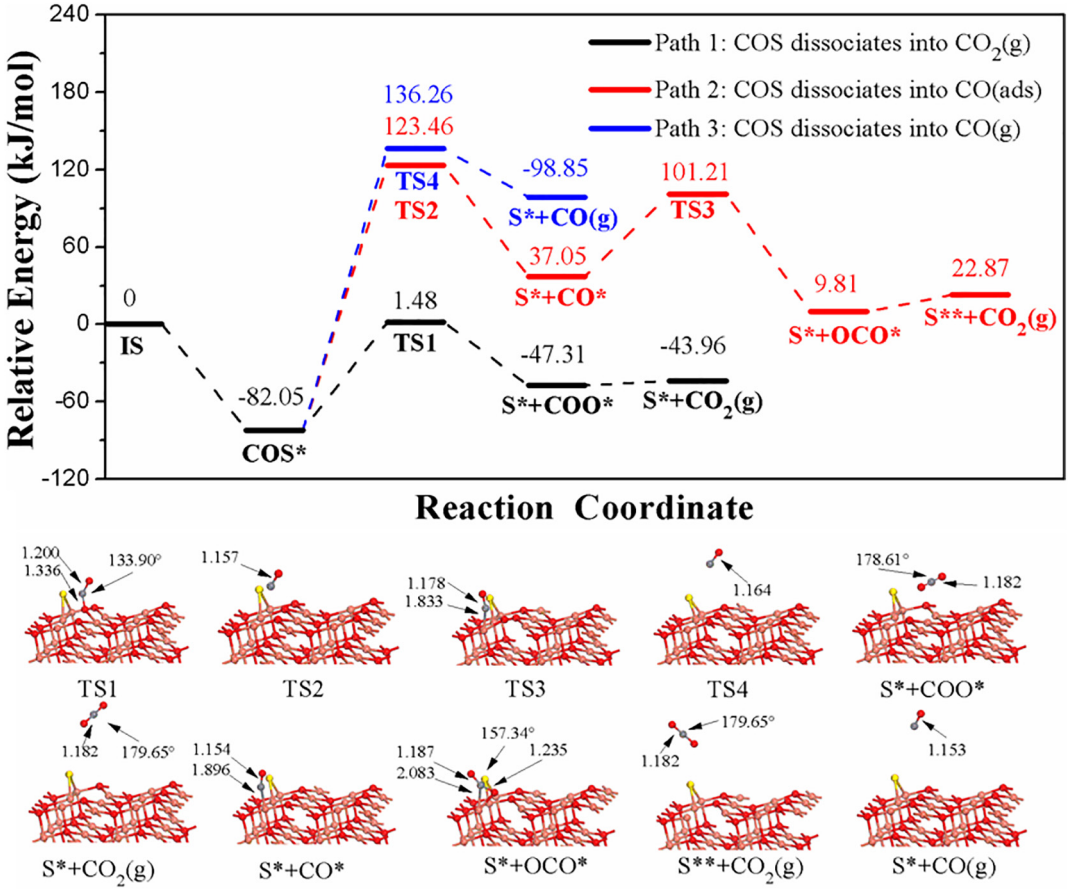

Fig. 7. Potential energy profiles and the corresponding structures of COS dissociation on the perfect CuO surface.

CO individual oxidation (27.98 kJ/mol), indicating that the presence of sulfur can significantly restrain the reaction activity of CO oxidation. The release of CO_2 is endothermic by −13.06 kJ/mol.

Path 3 (COS dissociates into CO(g), blue line): with the S—C bond cleavage, the (C—O)* group would migrate to above the surface with a distance of 5 Å, and produce a gaseous CO molecule. This elementary step is also a strongly endothermic reaction (180.90 kJ/mol) with an energy barrier of 218.31 kJ/mol at TS4. In this regard, both path 2 and path 3 of COS dissociation are difficult to take place, indicating that the formation of CO cannot be directly produced from COS dissociation on the perfect surface. However, above three paths of COS decomposition are too difficult to occur kinetically and thermodynamically.

3.5. The dissociation of COS on the defect surface

In view of the results presented in Section 3.4, only C—S bond cleavage is considered for the investigation of the COS decomposition on the defect surface in this section. Similarly, there are also three paths for COS decomposition, and potential energy profiles and the corresponding structures are depicted in Fig. 8.

Path 1 (COS dissociates into CO_2(g), black line): as the bond length of S—C is stretched from 1.8 Å to 3.0 Å, the (C—O)* group bonding to the T_{O3f} site can spontaneously produce an (O-C-O)* structure, as shown in Fig. 8 (S_{3f} + COO*). Unlike the perfect surface, the angle of the (O-C-O)* is 138.78°, and the sulfur atom stably fills into the defect site, while the carbon atom bonds tightly to the adjacent T_{Cu4f} site with a distance of 2.020 Å. The transient state has been searched and presented in Fig. 8 (TS1). The angle of the (O-C-O)* is 121.20°, which is also obviously smaller than the angle of free CO_2 (180°). The energy barrier of this step is 31.45 kJ/mol, which is lower than that of the perfect surface, indicating that the presence of oxygen vacancy immensely facilitates the reactivity of CO_2 generation. The release of CO_2 is endothermic by 10.27 kJ/mol.

Path 2 (COS dissociates into CO(ads), red line): with the S—C bond cleavage, the (C—O)* group would bond to the T_{Cu3f} site and form a configuration of CO adsorption. This elementary step is an endothermic reaction (34.48 kJ/mol) with an energy barrier of 84.86 kJ/mol at TS2. The relatively lower energy barrier (than that of the perfect surface) implies that the presence of oxygen vacancy can facilitate the generation of CO. Furthermore, the energy barrier of path 2 (84.86 kJ/mol) is higher than that of path 1 (31.45 kJ/mol), indicating that the formation of CO_2 (Path 1) is a more preferable pathway than the formation of CO (Path 2) on the defect surface. As for the subsequent oxidation of CO, CO interacts with the lattice oxygen atom and forms a surface linear CO_2 complex with an energy barrier of 46.33 kJ/mol at TS3, leading to the spontaneous release of gaseous CO_2.

Path 3 (COS dissociates into CO(g), blue line): with the S—C bond cleavage, the (C—O)* group produces a gaseous CO. This elementary step is also an intensively endothermic process (37.38 kJ/mol) with an energy barrier of 272.49 kJ/mol at TS4, indicating that the formation of gaseous CO cannot be directly produced from COS decomposition on the defect surface. Compared with the above three paths, it is found that the formation of CO_2 (Path 1) is a more preferable pathway than the formation of CO (Path 2), while gaseous CO can never be directly produced from COS dissociation (Path 3).

4. Discussion

The above calculation results suggest that the interaction of H_2S, HS*, and atomic S* with CuO will be enhanced as the dehydrogenation reactions proceed. Moreover, the adsorption of H_2S would promote the cleavage of H—S bond and the formation of O—H bond, which are in

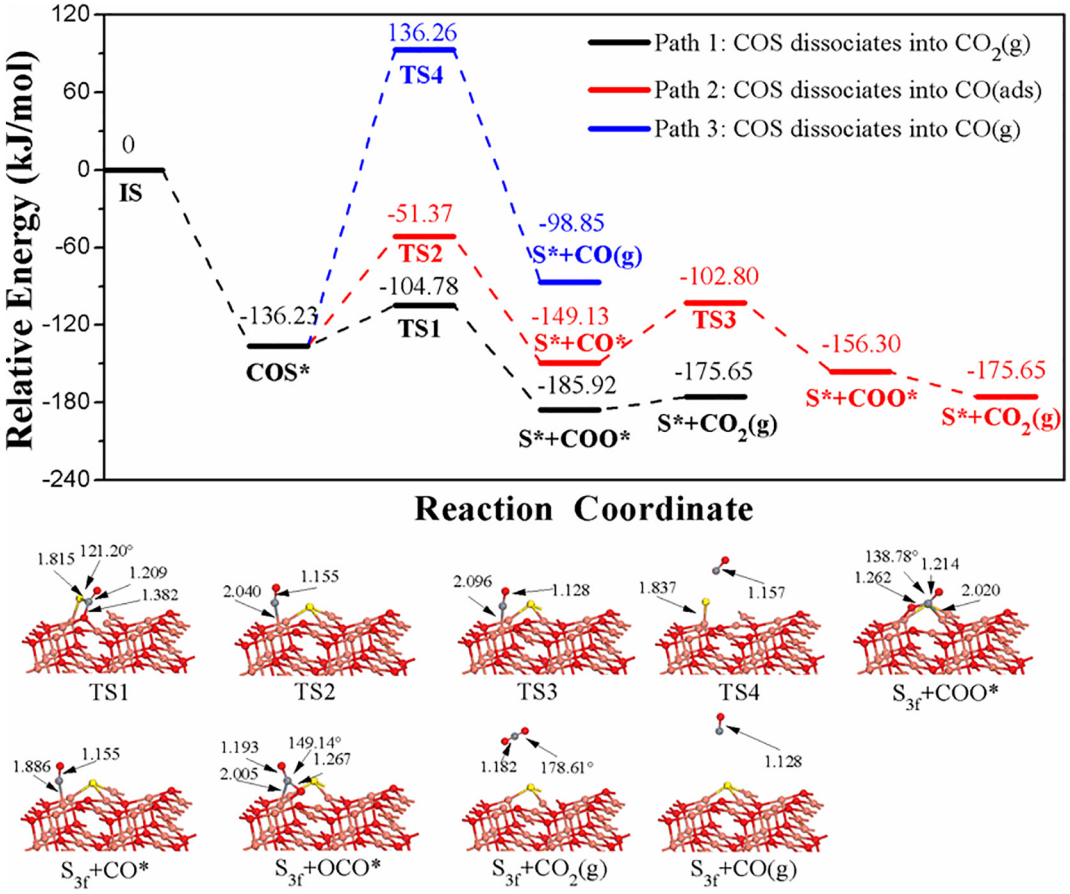

Fig. 8. Potential energy profiles and the corresponding structures of COS dissociation on the defect CuO surface.

line with previous results [23,24]. As shown in Fig. 3, the elementary reaction of H_2O formation is the rate-determining step in the whole reaction of H_2S + CuO → Cu_xS + H_2O, and the gaseous H_2 cannot be produced in this process (as shown in Fig. 4). Combining the results shown in Figs. 3 and 6, it is found that on the perfect and defect surfaces, HS* species would always be an active intermediate in both the dissociation and dehydration reactions for its activated hydrogen, and it plays a key role in multiple elementary reactions, which confirms the previous experimental results [48]. To be more specific, HS* species can not only dissociate into S* and H* but also contribute to the generation of H_2O via one-step reaction. That is, on the perfect surface, HS* species would be inclined to separate its H* atom to generate H_2O via one-step elementary reaction, rather than the two-step dissociation process on the basis of the energy barrier analyses. On the defect surface, the reaction of HS_{3f} + H* → S_{3f} + HOH* is also more easily to occur than the sub-step dissociation, both thermodynamically and kinetically. Since HS* species can be easily generated from the first step of H_2S dehydrogenation on both the perfect and defect surfaces, it might be crucially considered in the future study on the intrinsic kinetics and reaction mechanism among various sulfur-containing intermediates or products.

DFT results indicate that COS possesses strong adsorption capacity on the perfect and defect surfaces. The C—S bond cleavage is more favorable than the C—O bond cleavage, indicating that S atom (in COS molecule) has a stronger adsorption than that of C atom (in COS molecule). In addition, the adsorption energy of COS is higher than that of CO (49.2 kJ/mol) [18], both of which indicate that CO might take in a disadvantage status in the competition reaction under the sulfur-containing conditions. Furthermore, the surface structure can greatly affect the adsorption and dissociation characteristics and behaviors of COS molecule. Fig. 7 indicates that on the perfect surface, three pathways of the COS decomposition are difficult to take place due to both thermodynamic and kinetic factors, while the presence of oxygen vacancy is remarkably beneficial for the adsorption and subsequent decomposition. On the defect surface, the lowest energy barrier (31.45 kJ/mol) indicates that the formation of CO_2 is a preferable pathway than the formation of CO, indicating that COS mainly reacts with CuO directly via the heterogeneous reaction of COS + CuO → Cu_xS + CO_2. It might indicates that the reaction activity between COS and CuO is rather low in the initial stage of the reaction process. The oxygen carrier will generate many surface defects along with the proceeding of reaction process, and the reactivity of COS will be significantly increased accordingly.

In summary, it can be found that the dissociations of H_2S and COS will both lead to the generation of residual S* on the CuO surface, which would then produce copper sulfides (Cu_xS) as more dissociated S* atoms gather. It should be noted that only the dissociations of individual H_2S or COS molecules were investigated in this study, and we cannot make clear the detailed growth of the sulfides or identify the specific components (Cu_2S or CuS) layer by layer. The specific components of the surface and bulk region during the growth of sulfides might need further investigations, as in previous studies [41,49]. However, in terms of the sulfur fate, we examine three-step reaction of SO_2 formation from the residual S*, and Fig. 5 indicates that the energy barriers of SO_2 formation are rather high. It is thus speculated that gaseous O_2 is required to provide oxygen source for SO_2 formation, which can greatly reduce the energy barrier of the rate-limiting step of the sulfur oxidation process. This might be a possible explanation for that SO_2 can be more easily generated in the AR rather than FR [10,12,15], due to the large amount of gaseous oxygen in the AR. Note that, SO_2 can also be generated in the FR under the context of the chemical looping with oxygen uncoupling (CLOU), where gaseous O_2

will be released by the oxygen carrier in the FR condition. Furthermore, the activity of SO_2 formation might also be enhanced by the modification of multiple composite materials, which should be concretely evaluated on a case by case basis. That is to say, generally, the sulfidation process (forming Cu_xS) might be more likely to proceed in the FR, while the sulfur oxidation process (forming SO_2) is favored in the AR.

5. Conclusions

This study investigates the reaction mechanisms of sulfur-containing molecules (H_2S and COS) on the perfect and defect CuO (111) surfaces, including the complete process of adsorption, dissociation, and further reactions of H_2S or COS molecules. Both H_2S and COS strongly chemisorb at the CuO surface, and the surface structure can greatly affect the adsorption and dissociation characteristics of COS and H_2S. The main conclusions are as follows:

As for H_2S, it favorably adsorbs at the three-fold coordinated top copper site on the perfect and defect surfaces. The reaction of HS* → H* + S* is the rate-determining step in the two-step dissociation process, and the formation of H_2O is however the rate-determining step in the whole process. In terms of the defect surface, the adsorption of H_2S is greatly enhanced in the presence of oxygen vacancy. Meanwhile, HS* species is still an active intermediate, and the reaction of H_2O formation is a more preferable pathway than the dissociation reaction. Additionally, H_2 will never be produced during this process.

In view of COS, it favorably adsorbs at the hollow site $H_{Cu3f\text{-}Cu3f\text{-}O3f\text{-}O3f}$ on the perfect and defect surfaces. The results indicate that during the COS decomposition process, C—S bond activation is energetically more favorable than the C—O bond activation, leading to the formation of CO* or (O-C-O)* groups, and which would release as gaseous CO or CO_2 in the next step. On the perfect surface, the energy barriers of three paths of COS decomposition are too high, and thus are difficult to take place. In terms of the defect surface, the formation of CO_2 from COS decomposition is thermodynamically and kinetically more favorable. Namely, the formed surface defects during the CLC reduction process will immensely promote the direct reaction between COS and CuO.

Finally, the dissociations of H_2S and COS will all lead to the generation of residual S* on the CuO surface, which mainly exists in the form of S_{3f} site on the CuO surface. To investigate the sulfur evolution, the three-step sulfur oxidation with surface lattice oxygen is conducted, and sulfur secondary oxidation of (S—O)* → (O-S-O)* is the rate-determining step in the SO_2 formation process. Under O_2-free conditions, the sulfidation process might be more likely to proceed, and copper sulfides will generate as the dissociations of H_2S or COS proceed in the FR, while the sulfur oxidation is prone to occur in the AR.

CRediT authorship contribution statement

Chaohe Zheng: Conceptualization, Methodology, Validation, Formal analysis, Investigation, Data curation, Writing - original draft, Writing - review & editing. **Haibo Zhao**: Conceptualization, Resources, Writing - original draft, Writing - review & editing, Visualization, Supervision, Project administration, Funding acquisition.

Declaration of Competing Interest

The authors declare no competing financial interest.

Acknowledgment

These authors were supported by “National Key Research and Development Program of China (2016YFB0600801)” and “National Science Foundation of China (51522603)”.

Appendix A. Supplementary data

Supplementary data to this article can be found online at https://doi.org/10.1016/j.fuproc.2020.106431.

References

[1] C.R. Forero, P. Gayán, L.F. de Diego, A. Abad, F. García-Labiano, J. Adánez, Syngas combustion in a 500 W_{th} chemical-looping combustion system using an impregnated Cu-based oxygen carrier, Fuel Process. Technol. 90 (2009) 1471–1479.
[2] F. Liu, L. Yang, C. Song, Chemical looping hydrogen production using activated carbon and carbon black as multi-function carriers, Int. J. Hydrogen Energ. 43 (2018) 5501–5511.
[3] H. Zhao, X. Tian, J. Ma, M. Su, B. Wang, D. Mei, Development of tailor-made oxygen carriers and reactors for chemical looping processes at Huazhong University of Science & Technology, Int. J. Greenh. Gas Con. 93 (2019) 102898.
[4] F. Liu, X. Wu, L. Yang, H. Bu, X. Zhang, Evaluation of a bauxite cement-bonded Fe-based oxygen carrier during a hundred of cycles under coal-fueled chemical looping combustion conditions, Fuel Process. Technol. 199 (2020) 106267.
[5] D. Mei, A. Abad, H. Zhao, J. Adánez, Characterization of a sol–gel derived CuO/$CuAl_2O_4$ oxygen carrier for chemical looping combustion (CLC) of gaseous fuels: relevance of gas–solid and oxygen uncoupling reactions, Fuel Process. Technol. 133 (2015) 210–219.
[6] P. Moldenhauer, M. Rydén, T. Mattisson, A. Lyngfelt, Chemical-looping combustion and chemical-looping with oxygen uncoupling of kerosene with Mn- and Cu-based oxygen carriers in a circulating fluidized-bed 300W laboratory reactor, Fuel Process. Technol. 104 (2012) 378–389.
[7] T. Xin, M. Su, H. Zhao, Kinetics of redox reactions of CuO@TiO_2-Al_2O_3 for chemical looping combustion and chemical looping with oxygen uncoupling, Combust. Flame 213 (2020) 255–267.
[8] J. Ma, C. Wang, H. Zhao, X. Tian, Sulfur fate during the lignite pyrolysis process in a chemical looping combustion environment, Energ. Fuel 32 (2018) 4493–4501.
[9] B. Wang, R. Yan, D.H. Lee, D.T. Liang, Y. Zheng, H. Zhao, et al., Thermodynamic investigation of carbon deposition and sulfur evolution in chemical looping combustion with syngas, Energ. Fuel 22 (2008) 1012–1020.
[10] C.R. Forero, P. Gayán, F. García-Labiano, L.F. de Diego, A. Abad, J. Adánez, Effect of gas composition in chemical-looping combustion with copper-based oxygen carriers: fate of sulphur, Int. J. Greenh. Gas Con. 4 (2010) 762–770.
[11] R.D. Solunke, G. Veser, Integrating desulfurization with CO_2-capture in chemical-looping combustion, Fuel 90 (2011) 608–617.
[12] I. Adánez-Rubio, A. Abad, P. Gayán, F. García-Labiano, L.F. de Diego, J. Adánez, The fate of sulphur in the Cu-based chemical looping with oxygen uncoupling (CLOU) process, Appl. Energ. 113 (2014) 1855–1862.
[13] K. Wang, X. Tian, H. Zhao, Sulfur behavior in chemical-looping combustion using a copper ore oxygen carrier, Appl. Energ. 166 (2016) 84–95.
[14] X. Tian, K. Wang, H. Zhao, M. Su, Chemical looping with oxygen uncoupling of high-sulfur coal using copper ore as oxygen carrier, P. Combust. Inst. 36 (2016) 3381–3388.
[15] R.F. Pachler, K. Mayer, S. Penthor, M. Kollerits, H. Hofbauer, Fate of sulfur in chemical looping combustion of gaseous fuels using a copper-based oxygen carrier, Int. J. Greenh. Gas Con. 71 (2018) 86–94.
[16] T.T.M. Tran, C. Fiaud, E.M.M. Sutter, Oxide and sulphide layers on copper exposed to H_2S containing moist air, Corros. Sci. 47 (2005) 1724–1737.
[17] Genoveva Buelna, S.Y. Lin, Characteristics and desulfurization-regeneration properties of sol-gel-derived copper oxide on alumina sorbents, Sep. Purif. Technol. 39 (2004) 167–179.
[18] B.-X. Yang, L.-P. Ye, H.-J. Gu, J.-H. Huang, H.-Y. Li, Y. Luo, A density functional theory study of CO oxidation on CuO_{1-x}(111), J. Mol. Model. 21 (2015) 195.
[19] S. Sun, C. Li, D. Zhang, Y. Wang, Density functional theory study of the adsorption and dissociation of O_2 on CuO(111) surface, Appl. Surf. Sci. 333 (2015) 229–234.
[20] G. Hao, R. Zhang, J. Li, B. Wang, Z. Qiang, Insight into the effect of surface structure on H_2 adsorption and activation over different CuO(1 1 1) surfaces: a first-principle study, Comput. Mater. Sci. 122 (2016) 191–200.
[21] J. Zhang, R. Zhang, B. Wang, L. Ling, Insight into the adsorption and dissociation of water over different CuO(111) surfaces: the effect of surface structures, Appl. Surf. Sci. 364 (2016) 758–768.
[22] R. Zhang, H. Liu, J. Li, L. Ling, B. Wang, A mechanistic study of H_2S adsorption and dissociation on Cu_2O(111) surfaces: thermochemistry, reaction barrier, Appl. Surf. Sci. 258 (2012) 9932–9943.
[23] S. Sun, D. Zhang, C. Li, Y. Wang, DFT study on the adsorption and dissociation of H_2S on CuO(111) surface, RSC Adv. 5 (2015) 21806–21811.
[24] J. Zhang, M. Liu, R. Zhang, B. Wang, Z. Huang, Insight into the properties of stoichiometric, reduced and sulfurized CuO surfaces: structure sensitivity for H_2S adsorption and dissociation, Mol. Catal. 438 (2017) 130–142.
[25] J. Song, X. Niu, L. Ling, B. Wang, A density functional theory study on the interaction mechanism between H_2S and the α-Fe_2O_3(0001) surface, Fuel Process. Technol. 115 (2013) 26–33.
[26] C. Lin, W. Qin, C. Dong, H_2S adsorption and decomposition on the gradually reduced α-Fe_2O_3(001) surface: a DFT study, Appl. Surf. Sci. 387 (2016) 720–731.
[27] Y. Feng, X. Cai, X. Guo, C. Zheng, Influence mechanism of H_2S on the reactivity of Ni-based oxygen carriers for chemical-looping combustion, Chem. Eng. J. 295 (2016) 461–467.
[28] L. Ling, R. Zhang, P. Han, B. Wang, DFT study on the sulfurization mechanism during the desulfurization of H_2S on the ZnO desulfurizer, Fuel Process. Technol.

106 (2013) 222–230.
[29] X. Song, P. Ning, C. Wang, K. Li, L. Tang, X. Sun, et al., Research on the low temperature catalytic hydrolysis of COS and CS_2 over walnut shell biochar modified by Fe–Cu mixed metal oxides and basic functional groups, Chem. Eng. J. 314 (2017) 418–433.
[30] X. Sun, H. Ruan, X. Song, L. Sun, K. Li, P. Ning, et al., Research into the reaction process and the effect of reaction conditions on the simultaneous removal of H_2S, COS and CS_2 at low temperature, RSC Adv. 8 (2018) 6996–7004.
[31] S. Xin, N. Ping, W. Chi, L. Kai, H. Ruan, Research on the low temperature catalytic hydrolysis of COS and CS_2 over walnut shell biochar modified by Fe–Cu mixed metal oxides and basic functional groups, Chem. Eng. J. 314 (2016) 418–433.
[32] X. Song, P. Ning, C. Wang, K. Li, L. Tang, X. Sun, Catalytic hydrolysis of COS over CeO_2 (110) surface: a density functional theory study, Appl. Surf. Sci. 414 (2017) 345–352.
[33] X. Song, C. Wang, K.A.M. Gasem, K. Li, X. Sun, P. Ning, et al., New insight into the reaction mechanism of carbon disulfide hydrolysis and the impact of H_2S with density functional modeling, New J. Chem. 43 (2019).
[34] R. Zhang, L. Ling, B. Wang, Density functional theory analysis of carbonyl sulfide hydrolysis: effect of solvation and nucleophile variation, J. Mol. Model. 18 (2012) 1255–1262.
[35] J. Yu, L. Chang, W. Xie, D. Wang, Correlation of H_2S and COS in the hot coal gas stream and its importance for high temperature desulfurization, Korean J. Chem. Eng. 28 (2011) 1054–1057.
[36] L.-G. Gao, X.-L. Song, Y.-C. Wang, H.-Q. Wang, Theoretical study of the reaction of Cu^+ with OCS, J. Mol. Struc-Theochem. 810 (2007) 39–45.
[37] J.A. Rodriguez, J.C. Hanson, A.I. Frenkel, J.Y. Kim, M. Pérez, Experimental and theoretical studies on the reaction of H_2 with NiO: role of O vacancies and mechanism for oxide reduction, J. Am. Chem. Soc. 124 (2002) 346–354.
[38] J.P. Perdew, J.A. Chevary, S.H. Vosko, K.A. Jackson, M.R. Pederson, D.J. Singh, et al., Atoms, molecules, solids, and surfaces: applications of the generalized gradient approximation for exchange and correlation, Phys. Rev. B 46 (1992) 6671–6687.
[39] J.P. Perdew, K. Burke, M. Ernzerhof, Generalized gradient approximation made simple, Phys. Rev. Lett. 77 (1996) 3865–3868.
[40] Y. Zhang, H. Zhao, L. Guo, C. Zheng, Decomposition mechanisms of Cu-based oxygen carriers for chemical looping with oxygen uncoupling based on density functional theory calculations, Combust. Flame 162 (2015) 1265–1274.
[41] M. Su, J. Cao, X. Tian, Y. Zhang, H. Zhao, Mechanism and kinetics of Cu_2O oxidation in chemical looping with oxygen uncoupling, P. Combust. Inst. 37 (2019) 4371–4378.
[42] V.I. Anisimov, J. Zaanen, O.K. Andersen, Band theory and Mott insulators: Hubbard U instead of stoner I, Phys. Rev. B 44 (1991) 943–954.
[43] D. Wu, Q. Zhang, M. Tao, LSDA + U study of cupric oxide: electronic structure and native point defects, Phys. Rev. B 73 (2006) 235206.
[44] J. Hu, D. Li, J.G. Lu, R. Wu, Effects on electronic properties of molecule adsorption on CuO surfaces and nanowires†, J. Phys. Chem. C 114 (2010) 17120–17126.
[45] V. Massarotti, D. Capsoni, M. Bini, A. Altomare, A.G.G. Moliterni, X-ray powder diffraction *ab initio* structure solution of materials from solid state synthesis: the copper oxide case, Z. Kristallogr. 213 (1998) 259–265.
[46] Y. Maimaiti, M. Nolan, S.D. Elliott, Reduction mechanisms of the CuO(111) surface through surface oxygen vacancy formation and hydrogen adsorption, Phys. Chem. Chem. Phys. 16 (2014) 3036–3046.
[47] J. Paier, C. Penschke, J. Sauer, Oxygen defects and surface chemistry of ceria: quantum chemical studies compared to experiment, Chem. Rev. 113 (2013) 3949–3985.
[48] A. Davydov, K.T. Chuang, A.R. Sanger, Mechanism of H_2S oxidation by ferric oxide and hydroxide surfaces, J. Phys. Chem. B 102 (1998) 4745–4752.
[49] Y. Yang, L. Jing, L. Feng, W. Zhen, Z. Zhen, Comprehensive evolution mechanism of SO_x formation during pyrite oxidation, P. Combust. Inst. 37 (2019) 2809–2819.